Circulating extracellular vesicles derived from tumor endothelial cells hijack the local and systemic anti-tumor immune response: Role of mTOR/ G-CSF pathway

Malvina Koni [a,1], Tatiana Lopatina [a,1], Cristina Grange [a,1], Alessandro Sarcinella [a], Massimo Cedrino [b], Stefania Bruno [a], Fabrizio Buffolo [a], Saveria Femminò [a], Giovanni Camussi [a], Maria Felice Brizzi [a,*]

[a] Department of Medical Sciences, University of Turin, Turin, Italy
[b] 2i3T Scarl University of Turin, Via Nizza 52, Turin, Italy

ARTICLE INFO

ABSTRACT

Circulating tumour-derived extracellular vesicles are supposed to contribute to the spreading of distant metastasis. In this study, we investigated the impact of circulating extracellular vesicles derived from tumour-endothelial cells (TEVs) in the expansion of the metastatic bulk. We focus on the role of immune cells in controlling this process using the 4T1 triple negative breast cancer (TNBC) syngeneic model.

4T1 cells were intravenously injected and exposed to circulating TEVs from day 7. The lung, spleen, and bone marrow (BM) were recovered and analysed. We demonstrated that circulating TEVs boost lung metastasis and angiogenesis. FACS and immunohistochemically analyses revealed a significant enrichment of Ly6G$^+$/F4/80$^+$/ CD11b$^+$ cells and Ly6G$^+$/F4/80$^-$/CD11b$^+$ in the lung and in the spleen, while Ly6G$^+$/F4/80$^-$/CD11b$^+$ in the BM, indicating the occurrence of a systemic and local immune suppression. TEV immune suppressive properties were further supported by the increased expression of PD-L1, PD-1, and iNOS in the tumour mass. In addition, *in vitro* experiments demonstrated an increase of CD11$^+$ cells, PD-L1$^+$ myeloid and cancer cells, upregulation of LAG3, CTLA4 and PD-1 in T-cells, release of ROS and NOS, and impaired T-cell-mediated cytotoxic effect in co-culture of TEVs-preconditioned PBMCs and cancer cells. Granulocyte-colony stimulating factor (G-CSF) level was increased *in vivo,* and was involved in reshaping the immune response. Mechanistically, we also found that mTOR enriched TEVs support G-CSF release and trigger the phosphorylation of the S6 (Ser235/236) mTOR downstream target. Overall, we provided evidence that circulating TEVs enriched in mTOR supported G-CSF release thereby granting tumour immune suppression and metastasis outgrowth.

1. Introduction

According to the World Health Organization (WHO), breast cancer (BC) is the most common cancer worldwide, accounting for more than 12 % of all new annual cancer diagnosis. Moreover, BC is the second cause of mortality in Europe and United States [1]. Triple negative breast cancer (TNBC) is defined by the lack of oestrogen receptor (ER), progesterone receptor (PR), and human epidermal growth factor

receptor 2 (HER2) expression and is associated with aggressive growth, high rate of metastasis, and poor prognosis compared to all BC sub-types [1].

Cancer progression highly depends on the capability of cancer cells to interact with other cell types and to adapt into the dynamic tumour microenvironment (TME) [2]. TME is a complex microenvironment composed not only by tumour cells but also by endothelial cells, stromal cells, innate and adaptive immune cells, each of which communicates among themselves through a network of growth factors, cytokines, chemokines, and extracellular vesicles (EVs) [3]. Small size (30–200 nm) and virtual stability allow EVs to move from their site of origin, the TME in cancer, to the circulation, thereby impacting cellular activities at distant sites [4]. In cancer, the TME itself hijacks the EV cargo, like lipids, proteins, coding and non-coding RNAs (*e.g.* miRNAs and lnRNAs) to facilitate the multi-step metastatic process [4]. Angiogenesis, cancer cell homing, and tumor immune editing have also been attributed to tumor derived EVs.

Tumour-derived EVs are involved in both tumour specific and non-specific immune responses [5]. Although originally described as potential drivers of the anti-tumour immune response, several evidence provides insights on their role in hampering T-cell, natural killer and dendritic cell activation, while promoting the expansion of T-reg, myeloid derived suppressor cells (MDSCs), and T-cell exhaustion [6]. T-cell exhaustion was first described as an immune disorder [7]. Currently, exhausted T-cells are widely described as an immunosuppression mechanism accounting for tumor evasion [8]. T-cells, chronically exposed to programmed death-ligand 1 (PD-L1) on tumor and immune cells express inhibitory receptors (IRs), such as programmed death-1 (PD-1), cytotoxic T-lymphocyte antigen 4 (CTLA4) and lymphocyte activation gene 3 (LAG3), steadily lose their cytotoxic action [9]. T-cell exhaustion could be managed by MDSCs, characterized by the expression of Ly6G and CD11b, among other markers [10]. Immunosuppressive macrophages recognized by the expression of Ly6G, and F4/80 and CD11b, were also described [11].

Tumour endothelial cells (TECs) allow immune cell entrance into the TME and malignant cell entry into the circulation to reach secondary sites [12]. TECs display distinctive features and differ from normal endothelial cells in terms of surface protein expression, proliferation, and secretome, including EV cargo [13,14]. TECs and their released EVs (TEVs) share several properties. We have recently demonstrated in a xenograft model that circulating TEVs boost tumour vessel growth [15], while promote lung and liver metastases [16], and modulate the expression of PD-L1 on mononuclear cells, thereby dictating the tumour fate [17,18]. The impact of tumour cell-derived EVs in changing the TME has been deeply investigated, while the role of circulating TEVs in governing the immune response at distant sites still lack robust evidence.

In this study, we aimed to investigate the role of circulating TEVs in the establishment of a tumour supportive milieu and their impact on the systemic and local immune responses.

2. Material and methods

2.1. Cell cultures

The 4T1 cell line was purchased from ATCC and cultured in RPMI 1640 (Euroclone) supplemented with 10 % FBS (GIBCO). Human-derived TECs was obtained from surgical tumor specimens using anti-CD105-positive selection and grown in the complete EndoGro medium (Millipore) [19].

2.2. EV isolation and characterization

For TEV isolation, confluent TEC were cultured in serum-free DMEM (Euroclone) for 18 h. The conditioned medium was centrifuged for 30 min at 3000 g and filtered with 0.22 μm filters (Millipore) to remove cell debris and apoptotic bodies. After that the supernatant was ultra centrifuged for 2 h at 100,000 g at 4 °C (Beckman Coulter Optima L-100 K Ultracentrifuge, rotor type 45 Ti 45000RPM). TEV pellet was resuspended in PBS (Euroclone) supplemented with 1 % of DMSO and stored at − 80 °C for further use [17,18]. As control EVs recovered from serum of patients (3 different patients) without cancer and expressing high level of endothelial markers were used. Isolation and characterization were performed as previously reported [20,21].

TEVs were analysed using the Nanoparticle tracking analysis (NTA) by NanoSight NS300 system (Malvern Instruments, Ltd), transmission electron microscopy (Jeol 1140 Flash electron microscope, Jeol, Tokyo, Japan) and western blot analysis. For further characterization, flow cytometry analysis was performed using the MACSPlex Exosome Kit (Miltenyi Biotec), following the manufacturer's protocol [18]. Super-resolution microscopy acquisition of TEVs was performed using Nanoimager S Mark II microscope from ONI (Oxford Nanoimaging, Oxford, UK) equipped with a 100x, 1.4NA oil immersion objective, an XYZ closed-loop piezo 736 stage, and triple emission channels split at 640, 488 and 555 nm. The experiment was performed using EV profiler Kit (ONI) following manufacturer's protocol. The EV profiler Kit contains fluorescent antibodies anti CD9–488, CD63–568 and CD81–647. Images were taken in dSTORM mode acquired sequentially in total reflection fluorescence (TIRF) mode. Single-molecule data was filtered using NimOS software (v.1.18.3, ONI). Data has been processed with the Collaborative Discovery (CODI) online analysis platform www.alto.codi.bio from ONI and the drift correction pipeline version 0.2.3 was used [22].

2.3. Western blot

Western blot analysis for TEVs was performed under reducing conditions using a 10 % SDS–PAGE (BioRad) using 30 μg proteins/lane. Proteins were transferred to nitrocellulose membranes, saturated with 10 % BSA for 2 h and incubated with specific antibodies overnight at 4 °C. For detection peroxidase-conjugated secondary antibodies were used, the chemiluminescent ECL reagent and ChemiDoc™ XRS+ System (BioRad). The following anti-human antibodies were used: CD63 (abcam, #ab134045), CD81 (abcam, #ab109201), CD29 (Invitrogen, #Ma5–17103), GM-130 (abcam, #ab52649), CD9 (abcam, #ab92726), mTOR (Cell Signaling, #11/2015) and anti-human p-S6 ribosomal protein (Ser235/236) (Cell Signaling, #4858).

2.4. In-vivo metastasis model

Animal studies were conducted in accordance with the Italian National Institute of Health Guide for the Care and Use of Laboratory Animals (protocol # 518/2022-PR). Mice were housed according to the guidelines of the Federation of European Laboratory Animal Science Association and the Ethical Committee of the University of Turin.

Eight week-old female BALB/c mice were intravenously injected with 1.5×10^4 4T1 cells. After one-week, animals were treated with saline, circulating EVs recovered from patients without cancer, or TEVs, (1×10^{10}/injection, TEV number resulting for our previous investigation) at day 7–9–11–15 after 4T1 cell injection. At day 18 mice were sacrificed and sera, lung, spleen, and bone marrow were recovered for further analysis.

2.5. Mice sample processing and analysis of the immune cell infiltrate

For FACS analysis of immune cells, lung, spleen and bone marrow were collected. Lung and spleen tissue was first minced into a petri dish in small pieces and passed through 40 μm cell strainer using the back of a 2,5 ml syringe and PBS (Euroclone) in order to obtain a single cell solution. The samples were centrifuged 5 min at $25 \times g$, supernatants were removed, and the pellets resuspended in PBS 1 % BSA for immune staining. Red blood cell lysis was performed on spleen samples by

adding 1 ml of red blood cells lysis solution in each tube and incubated 5 min. All samples were therefore centrifuged 5 min at 25 x g and washed. Bone marrow cells were isolated from femur and tibia by flushing with 5 ml of DMEM supplemented with 5 % of non-enzymatic cell dissociation solution (Gibco). Then, the samples were centrifuged and resuspended in 2 ml of PBS 1 % BSA for immune staining and FACS analysis. A pool of approximately 5×10^6 cells was dissolved in 100 µl and incubated with antibodies and incubated 30 min at 4 °C in the dark. FITC, PerCP, ACP, VioBlue or PE non-immune isotypic IgG, or unstained control were used to normalise physical and electrical parameters and to design the gating strategy. The following antibodies were used for mix 1: CD45-APC (Cat#130–110–803), CD4-VioBlue (Cat#130–118–696), CD8-PerCP (Cat#130–123–240); for mix 2: CD45-APC (Cat#130–110–803), Ly6G-PE (Cat#130–123–780), F4/80-FITC (Cat#130–117–509), CD11b-VioBlue (Cat#130–113–810), all from Miltenyi Biotec. For data acquisition, CytoFLEX Flow Cytometer (Beckman Coulter) was used and data were analysed with Cytexpert software.

2.6. Immunohistochemistry

Immunohistochemistry was performed using an automated slide-processing platform (Ventana BenchMark AutoStainer, Ventana Medical Systems, Tucson, AZ, USA), with Universal DAB Detection Kit detection systems. 5-µm paraffin embedded lung sections were stained. Three or five sections/group were analysed using ImageJ software, and the results expressed as the percentage of positive area ± SEM. Quantifications of positive areas were performed using Fiji software.

The following antibodies were used: CD31 (abcam, #ab7388), PD-1 (abcam, #ab214421), PD-L1 (abcam #ab233482), CD11b (abcam #ab75476), iNOS (Biocompare, #A14031), F4/80 (abcam, #ab300421), Ly6G (abcam, #ab238132), CD83 (SantaCruz Biotechnology, #sc-55535) and CD8 (abcam, ab217344).

2.7. PBMC isolation and culture

Fresh PBMCs were isolated from healthy donors. The heparinized blood samples were used for the density gradient centrifugation. PBMCs were seeded in 24 well plates at a density of 2×10^6 cells per well in 2 ml of serum-free AIM V medium. The use of PBMC was approved by the Ethic Committee of A.O.U. Città della Salute e della Scienza di Torino, Turin, Italy (CS21255–Protocol # 0050416). TEVs were added to PBMCs at the concentration of 1×10^3/cell. Unstimulated PBMC served as control. After 48 h, PBMCs were analysed by FACS using the anti-human PD-1 (BD Pharmigen, #557946), LAG3 (Biolegend, #369306), CTLA4 (Biolgend, #349906), CD11b (Dako, #R0841) and PD-L1 (Biolegend, #329705).

For co-culture experiments, 4T1 cells were seeded in 24 well plates, at the concentration of 2×10^4/well. Meanwhile, freshly isolated PBMCs were stimulated with TEVs as above described for 24 h. Finally, pre-stimulated PBMCs were added to 4T1 cells for 48 h. As control, 4T1 cells co-cultured with unstimulated PBMCs were used. FACS analysis was performed using the aforementioned anti-human antibodies and the anti-mouse PD-L1 (Biolegend, #124334).

In selected experiments the anti-human G-CSF antibody was used (R&D System, #MAB214) at 0,6 µg/ml concentration, while rapamycin was used at the concentration of 50 nM (Selleckchem, #S1039).

2.8. Measurement of ROS production and NOS activity

The intracellular production of ROS was measured using the Muse oxidative stress kit (Millipore, #MCH100111), following manufacturer instructions. NO activity was detected by using the Nitric oxide assay kit (Millipore, #482650) according to manufacturer instructions.

2.9. ELISA Assay

ELISA assay was performed to investigate the presence of anti-human antibodies in mouse serum. For this purpose, TEVs were used as captured antigens. In total 10 µg of TEVs per well was used for coating the plate over night at RT. Serum from mice experiencing circulating TEVs, from control or healthy mice was analysed the day after. Anti-human mouse antibodies were detected using the peroxidase-conjugated secondary anti-mouse goat antibodies.

Relative quantification of human G-CSF (R&D Systems, #DY214), IL-1β (R&D Systems, #DY201) IL-10 (R&D Systems, #DY217B), and murine G-CSF (PeproTech, #900-M103) were performed according to manufacturer instructions.

2.10. miR screening

TEVs were analysed for their miRNA content by qRT–PCR by using the Applied Biosystems TaqManH MicroRNA Assay Human Panel Early Access kit (Life Technologies). Reverse transcription using Applied Biosystems 7900 H qRT–PCR instrument, as previously described [15] investigated the expression profile of 375 human mature miRNAs in TEVs. The evaluation of miRNAs expression was analysed using the Expression Suite software (Life Technologies). miRNA fold change was calculated as $2^{-\Delta\Delta Ct}$. The expression of miRNAs of importance was confirmed using the TaqMan microR specific assay kit (Applied Biosystems, Foster City, CA, USA).

2.11. Enriched miRNAs with RQ>10were selected for miRNA gene targeting and pathway analysis

miRNA target genes were retrieved by miRWalk2.0 database [23]. Validated miRNA gene targets from MiRTarBase were used for the following analysis [24]. Enriched "Reactome 2022" pathways were generated by testing MiRTarBase-derived gene sets with EnrichR (retrieved in March 2023) [25]. Adjustment of p-value for multiple testing was performed with Benjamini-Hochberg to calculate q-values. The pathway network and cluster analysis were performed with Gephi 0.9.2 and shows significantly enriched pathways (q<0.01). The nodes represent enriched pathways and the node size is proportional to – log (q value) of each pathway. Connection thickness is proportional to the number of overlapping genes, as calculated by Jaccard Index. Connections with Jaccard Index< 0.1 were excluded. Unbiased clustering of pathways was performed through modularity assessment [26]. Gene-pathway network analysis was performed for the community enriched in "immune system" pathways. In this presentation, gene-nodes representing the genes enriched in each specific pathway are connected to pathway-nodes of origin.

2.12. Phosphorylation assay

PBMCs were isolated as previously described and seeded in 24 well plates at the density of 2×10^6 cells per well in 2 ml of serum-free AIM V medium. TEVs (1×10^3/cell) and Rapamycin (50 nM) (Selleckchem, #S1039) were added to PBMCs. After 25 min, PBMCs were recovered, centrifuged, and immediately placed at 4 °C in RIPA lysis and Extraction Buffer (Thermo Scientific™ #89900) in the presence of 1X diluted Protease/Phosphatase Inhibitor Cocktail (Cell SignalingTechnology™ #5872) for 1 h. Protein phosphorylation was analysed by western blot.

2.13. Statistical analysis

All data are reported as mean ± SEM. Comparison between two groups was analysed out by Student's t-test while comparisons amid 3 or more groups have been performed using one-way ANOVA or followed by Tukey's multiple-comparison test or two-way ANOVA followed by Šídák's multiple comparisons test. *p*-value < 0.05 was considered as

significant. All *in vitro* and *in vivo* data are representative of at least 3 independent experiments. Graph Pad Prism (Graph Pad Software, 8.0.1 version) was used for all statistical analyses.

3. Results

### 3.1. TEVs increase lung metastasis formation and angiogenesis

Firstly, TEVs were characterized by TEM, NanoSight, MACSPlex and Western blot analyses (Supplementary Fig. S1). We have previously demonstrated that circulating TEVs may provide the "soil" for the recruitment and outgrowth of TNBC cells in the lung [16,18]. In the present study we aimed to investigate their role in boosting the outgrowth of lung metastases by systemically and/or locally shaping the immune system. To this purpose the murine mammary 4T1 cancer cell line was selected as syngeneic model [27]. Firstly, BALB/c mice intravenously injected with the 4T1 tumour cells were subjected to vehicle, TEVs, or EVs from patients without cancer starting from day 7 as indicated in the model (Fig. 1A). Macroscopic evaluation and histological analyses of the lung demonstrated the presence of massive metastatic nodules mostly in TEV exposed group, thereby corroborating that 4T1 cells forcefully expanded in the presence of circulating TEVs (Fig. 1B-D). Moreover, as shown by the CD31 staining, vascular density was also increased in the lung of these animals (Fig. 1D). Overall, these data demonstrated that circulating TEVs boost lung metastasis and expand

the vessel network in the lung of immunocompetent mice. No metastatic foci were found in the liver (Supplementary Fig. S2). Since no differences between vehicle and circulating EVs recovered from patients without cancer were found, vehicle was used as internal control throughout the study.

3.2. Circulating TEVs promote a strong systemic immune reaction involving the spleen and the bone marrow

The effect of TEVs on the immune activation was first evaluated by analysing the spleen. Our results showed a striking difference in the spleen size between mice exposed to circulating TEVs or saline. As shown in Fig. 2A, circulating TEV exposed mice displayed a significant increase of the spleen mass compared to control and healthy animals The average size of the spleen recovered from the TEV group was 2.3 ± 0.2 cm, compared to 1.7 ± 0.1 cm and 1.5 ± 0.1 cm of control and healthy group respectively, suggesting that circulating TEVs boosted a systemic immune reaction. We also tested the possibility that TEVs can induce a specific anti-TEV immune response. Serum recovered from healthy, control, and TEV exposed mice were analysed for the presence of anti-TEV specific antibodies. According to this analysis, we demonstrated that serum from TEV exposed animals was enriched of TEV-binding antibodies compared to healthy and control mice (Fig. 2B).

We next investigated the effect of circulating TEVs on the systemic immune response by examining the immune cell compartment in the
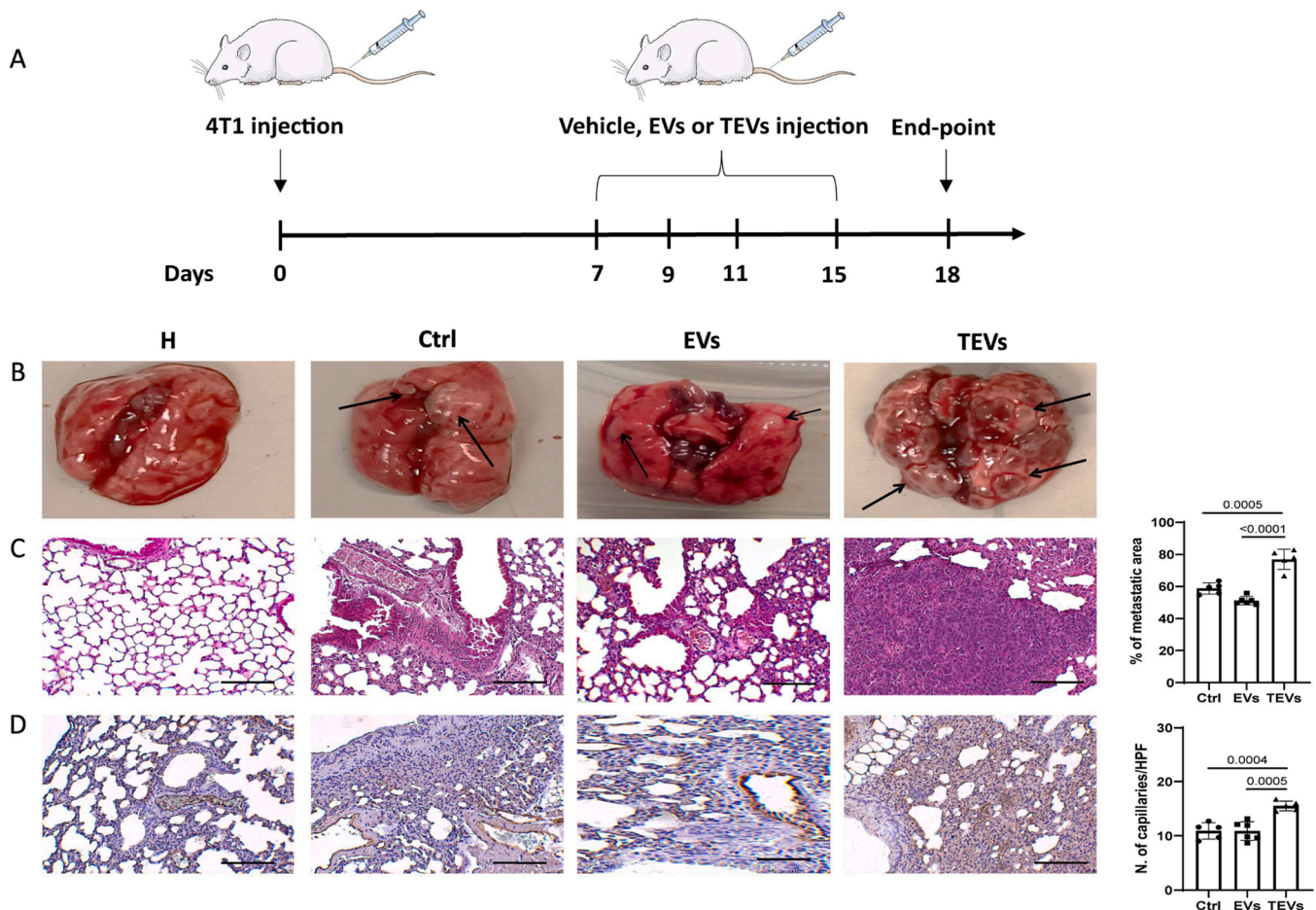
Fig. 1. Effects of circulating TEVs on metastasis outgrowth. (A) Schematic representation of the *in vivo* study. (B) Representative images of lungs obtained from healthy (H), saline (Ctrl), EVs isolated from serum of patients without cancer (EVs), or TEV mice (TEVs). (C) Representative images of lung metastasis derived from healthy (H), control (Ctrl), EVs and TEV mice (TEVs) stained with haematoxylin/eosin. Quantification of metastasis was expressed as the percentage of positive area/total area (D) Representative images of immune-histochemical staining for CD31 and quantification of lung capillaries in healthy (H), saline (Ctrl), EVs from patient's cancer free, and TEV mice (TEVs). Original magnification 20X, scale bar: 100 μm. Data are presented as the mean ± SEM (n = 3 or n = 5).
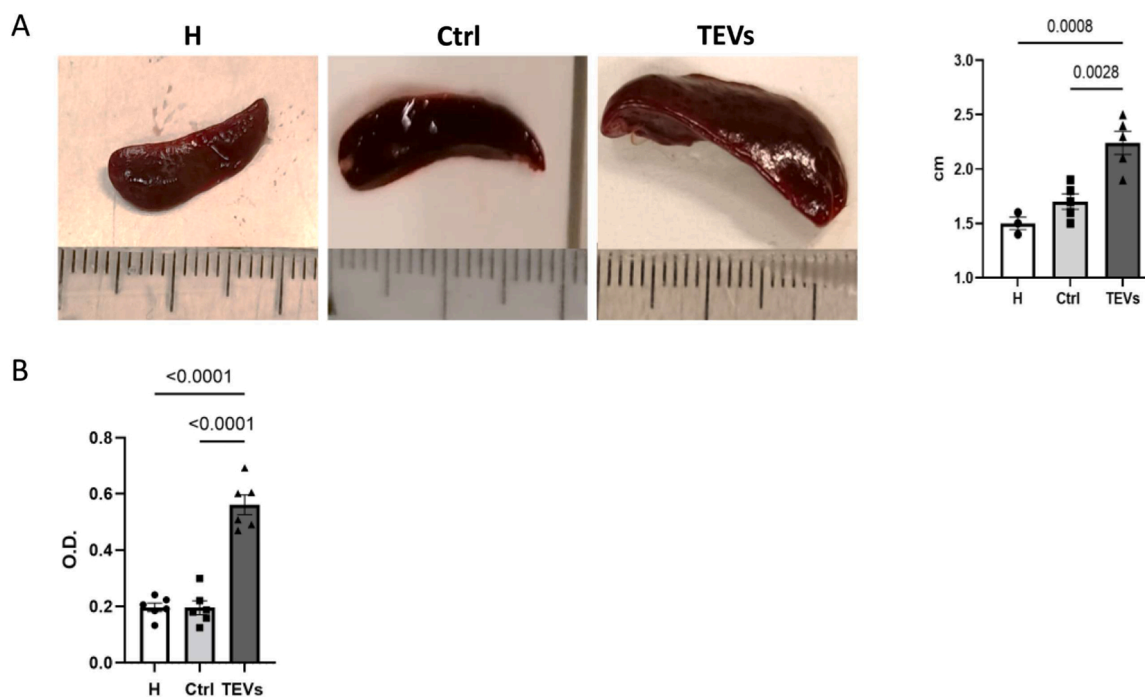
Fig. 2. Circulating TEVs induce systemic immune response. (A) Representative images of spleens recovered from healthy (H), saline (Ctrl) and TEV mice (TEVs). Their enlargement is expressed in cm. (B) ELISA assay was performed for the quantification of specific anti-TEV antibodies in mice. TEVs were used to coat the plate, and serum from different experimental conditions added to detect the presence of specific anti-TEV antibodies. Data are presented as the mean absorbance $\pm$ SEM (n = 3 or n = 6).

spleen and bone marrow. We demonstrated that circulating TEVs were able to significantly increase the number of MDSCs (Ly6G$^+$/F4/80$^-$/CD11b$^+$) both in the spleen and bone marrow, while Ly6G$^+$/F4/80$^+$/CD11b$^+$ cells only in the spleen (Fig. 3 and Fig. 4 respectively). No difference in the number of CD4$^+$ and CD8$^+$ cells was detected in the lung, spleen and bone marrow of mice exposed to circulating TEVs (Supplementary Fig. S3 and S4). Overall, these results indicate that circulating TEVs promote a systemic accumulation of myeloid immunosuppressive cells.

3.3. Circulating TEVs boost the recruitment of immune cells in the lung

Since circulating TEVs significantly increased the metastatic outgrowth, the lung immune microenvironment was also analysed and compared among the different experimental groups. Based on the pan immune CD45 cell marker, we found a significantly increase in their number in TEV exposed animals compared to control and healthy groups. Along with an increased CD45$^+$ cells, we also demonstrated that circulating TEVs significantly increase the amount of Ly6G$^+$/F4/80$^+$/CD11b$^+$ and Ly6G$^+$/F4/80$^-$/CD11b$^+$ cells (Fig. 5). Accumulation of Ly6G$^+$, F4/80$^+$, and CD11b$^+$ cells in the lung of mice exposed to circulating TEVs was also confirmed by immunohistochemistry (Fig. 6).

We have previously shown, in a xenograft model, that TEVs upregulate PD-L1 expression on tumour cells [18]. In this immunocompetent model we observed a significant increase of PD-L1 positive cells in the lung tissue of animals exposed to circulating TEVs (Fig. 7B). In addition, an increase number of PD-1$^+$ and CD83$^+$ cells [28,29] were found in the lung of these animals, suggesting that TEVs also suppress T-cell-mediated anti-tumour activities (Fig. 7A and C).

3.4. TEVs contribute to T-cell exhaustion

To confirm the *in vivo* immunosuppressive action of TEVs and to likely identify TEV mechanism of action on T-cells, firstly, PBMCs from healthy-donors were cultured with TEVs and evaluated for the

expression of PD-L1 and T-cell exhaustion markers. As shown in Fig. 8 TEVs induced the expression of PD-L1 in myeloid cells (Fig. 8A) and PD-1, LAG3, and CTLA4 in isolated T-cells (Fig. 8B). TEV-primed PBMCs were also co-cultured with 4T1 cells and both cell types were analysed for PD-L1 expression. Indeed, we found that in these experimental conditions PD-L1 expression was increased in both myeloid and 4T1 cells (Fig. 8D and G). Moreover, when T-cell exhaustion markers were analysed, we demonstrated the increased expression of all of them (Fig. 8E). Finally, consistent with the *in vivo* data, we demonstrated that TEVs expand CD11b$^+$ cells even in co-culture conditions (Fig. 8C and F). These findings confirm *in vitro* the immunosuppressive environment generated by TEVs.

Mitochondrial dysfunction and metabolic alteration reflect disorder of the redox homeostasis in cancer cells [30,31]. Several studies have shown that oxidative stress promotes tumour immune escape by creating an immunosuppressive TME [31]. iNOS was first evaluated in the lung. As shown in Fig. 6D, iNOS was increased in animals exposed to circulating TEVs. An increased NOS production was also detected in TEVs-preconditioned PBMCs (Supplementary Fig S2A). ROS generation was therefore evaluated in PMBCs preconditioned with TEVs, as well as in co-culture experiments. Notably, upon TEV administration an increase of ROS generation was detected in both experimental conditions (Supplementary Fig. S5B-C).

To functionally confirm the immunosuppression environment generated by TEVs, PBMC cytotoxic activity was evaluated in 4T1 cells. As expected, TEVs-primed PBMCs failed to exert their cytotoxic action (Supplementary Fig. S5D). Consistent with this observation we demonstrated that IL-10 and IL-1β are also increased (Supplementary Fig. S5E-F). Overall, these results further sustain the multifaceted immune suppression generated by TEVs.

3.5. G-CSF contributes to TEVs-mediated immune-suppression

It has been extensively demonstrated that human donors subjected to G-CSF administration increase the numbers of both monocyte and
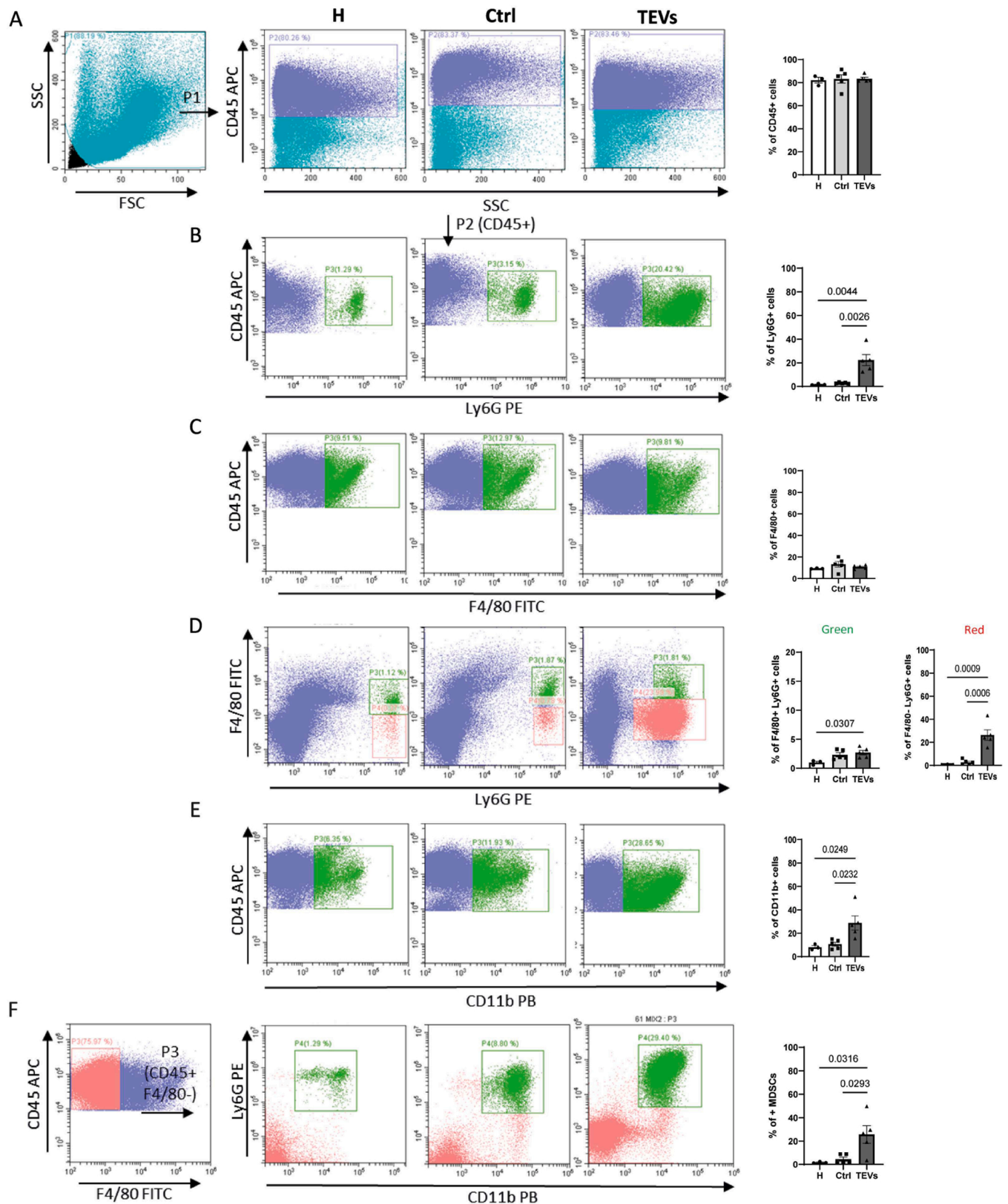
Fig. 3. Circulating TEVs drive MDSC accumulation in the spleen. Total mouse splenocytes from BALB/C mice were prepared as described in Materials and Methods. (A) Debris (SSC *vs*. FSC) were excluded (gate P1) and cells gated for the analysis of CD45$^+$ cells (P2). CD45$^+$ cells were sub-gated for further Ly6G$^+$ (B), F4/80$^+$ (C), F4/80$^+$/Ly6G$^+$ (green gate), F4/80$^-$/Ly6G$^+$ (red gate) (D), and CD11b$^+$ cells (E) characterization. MDSCs were gated as CD45$^+$/F4/80$^-$ (gate P3) and Ly6G$^+$/CD11b$^+$ cells (F). Data are presented as the mean ± SEM (n = 3 for healthy, n = 5 for experimental groups).
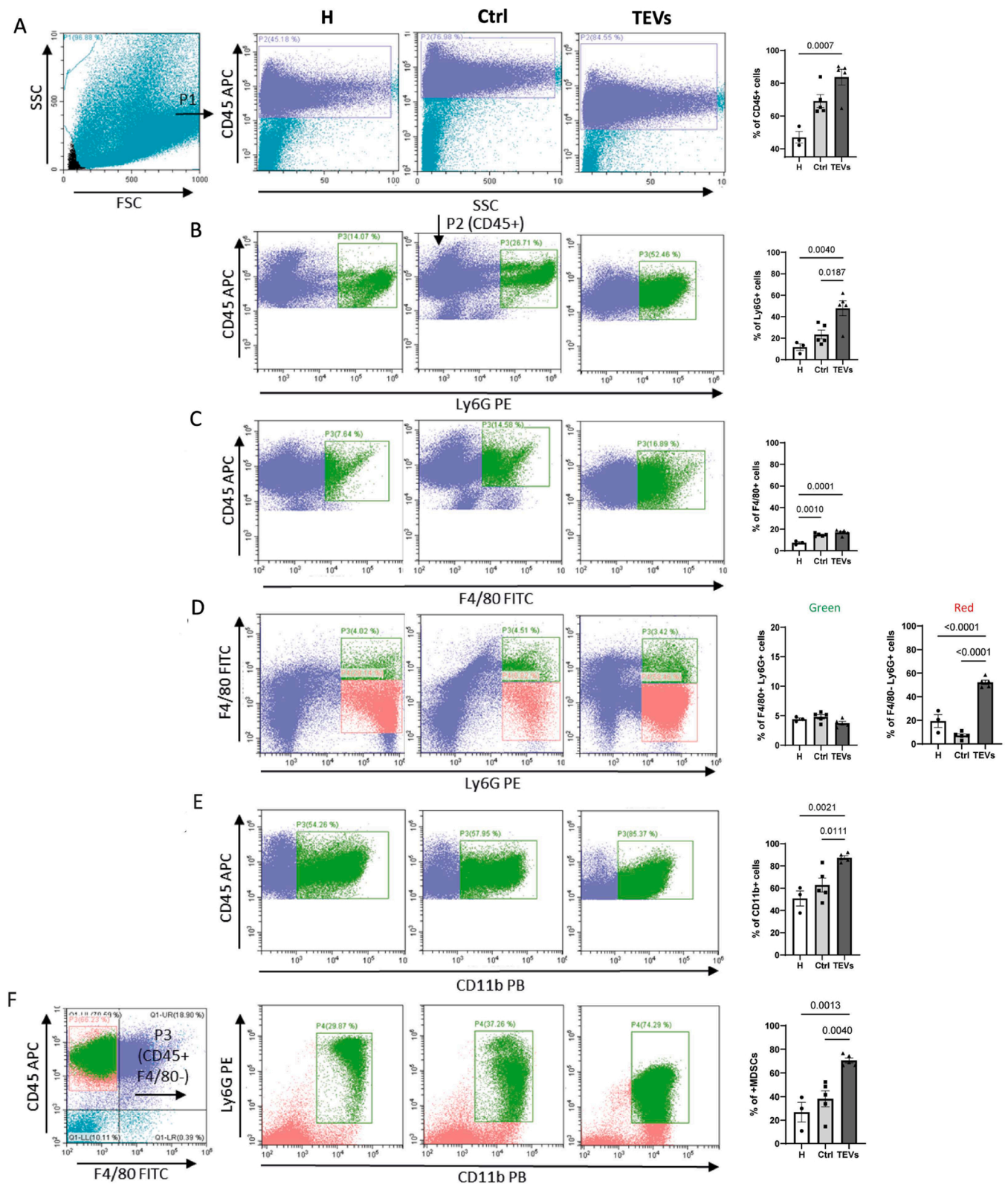
Fig. 4. Circulating TEVs induce Ly6G+ /F4/80-/CD11b+ cell accumulation of the bone marrow. Total mouse bone marrow cells from BALB/C mice were prepared as described in Materials and Methods. (A) Debris (SSC *vs.* FSC) were excluded (gate P1) and cells gated for the analysis of CD45$^+$ cells (P2). CD45$^+$ cells were sub-gated for further Ly6G$^+$ (B), F4/80$^+$ (C), F4/80$^+$/Ly6G$^+$ (green gate), F4/80$^-$/Ly6G$^+$ (red gate) (D), and CD11b$^+$ (E) characterization. MDSCs were gated as CD45$^+$/ F4/80$^-$ (gate P3) and Ly6G$^+$/CD11b$^+$ cells (**F**). Data are presented as the mean ± SEM (n = 3 for healthy, n = 5 for experimental groups).

7
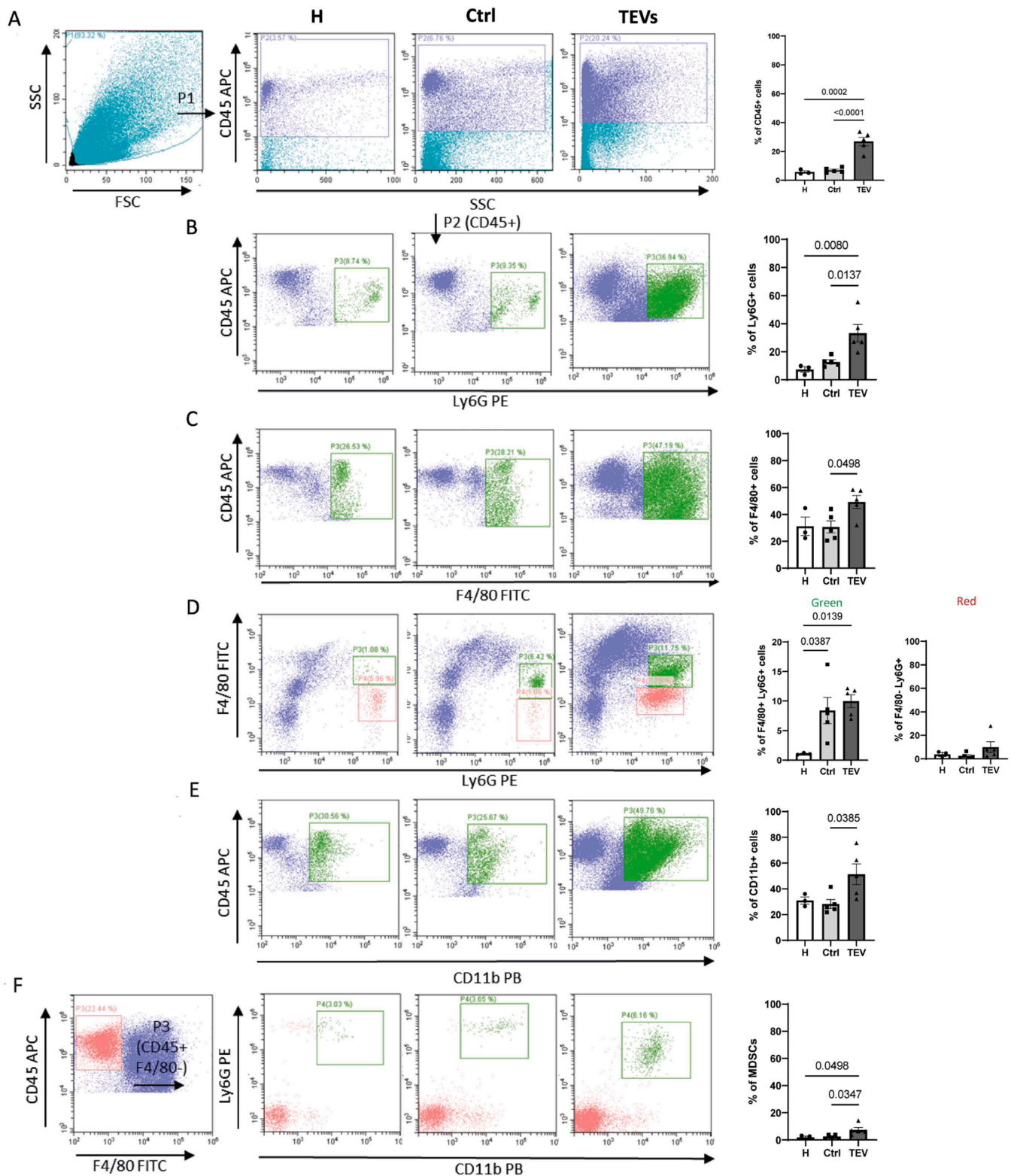
Fig. 5. Circulating TEVs account for MDSC accumulation in the lung. Total mouse lung cells from BALB/C mice were prepared as described in Materials and Methods. (A) Debris (SSC *vs.* FSC) were excluded (gate P1) and cells gated for the analysis of CD45$^+$ cells (P2). CD45$^+$ cells were sub-gated for further Ly6G$^+$ (B), F4/80$^+$ (C), F4/80$^+$/Ly6G$^+$ (green gate), and F4/80$^-$/Ly6G$^+$ (red gate) (D), and CD11b$^+$ (E) characterization. MDSCs were also gated as CD45$^+$/F4/80$^-$ (gate P3) and Ly6G$^+$/CD11b$^+$ cells (F). Data are presented as the mean ± SEM (n = 3 for healthy, n = 5 for experimental groups).

granulocytic MDSC subtypes [32]. In addition, G-CSF can induce T-cell transition from Th1 to Th2 phenotype, inhibit T-cell proliferation and promote apoptosis [33,34]. Therefore, we sought to determine whether G-CSF may contribute to TEVs-induced immune suppression. To this end, G-CSF was evaluated *in vivo,* in animals exposed to circulating TEVs, and *in vitro* in the conditioned media (CM) of PBMCs undergoing TEV preconditioning. As shown in Fig. 9A G-CSF was enriched in sera of animals exposed to circulating TEVs. Moreover, since TEVs may carry
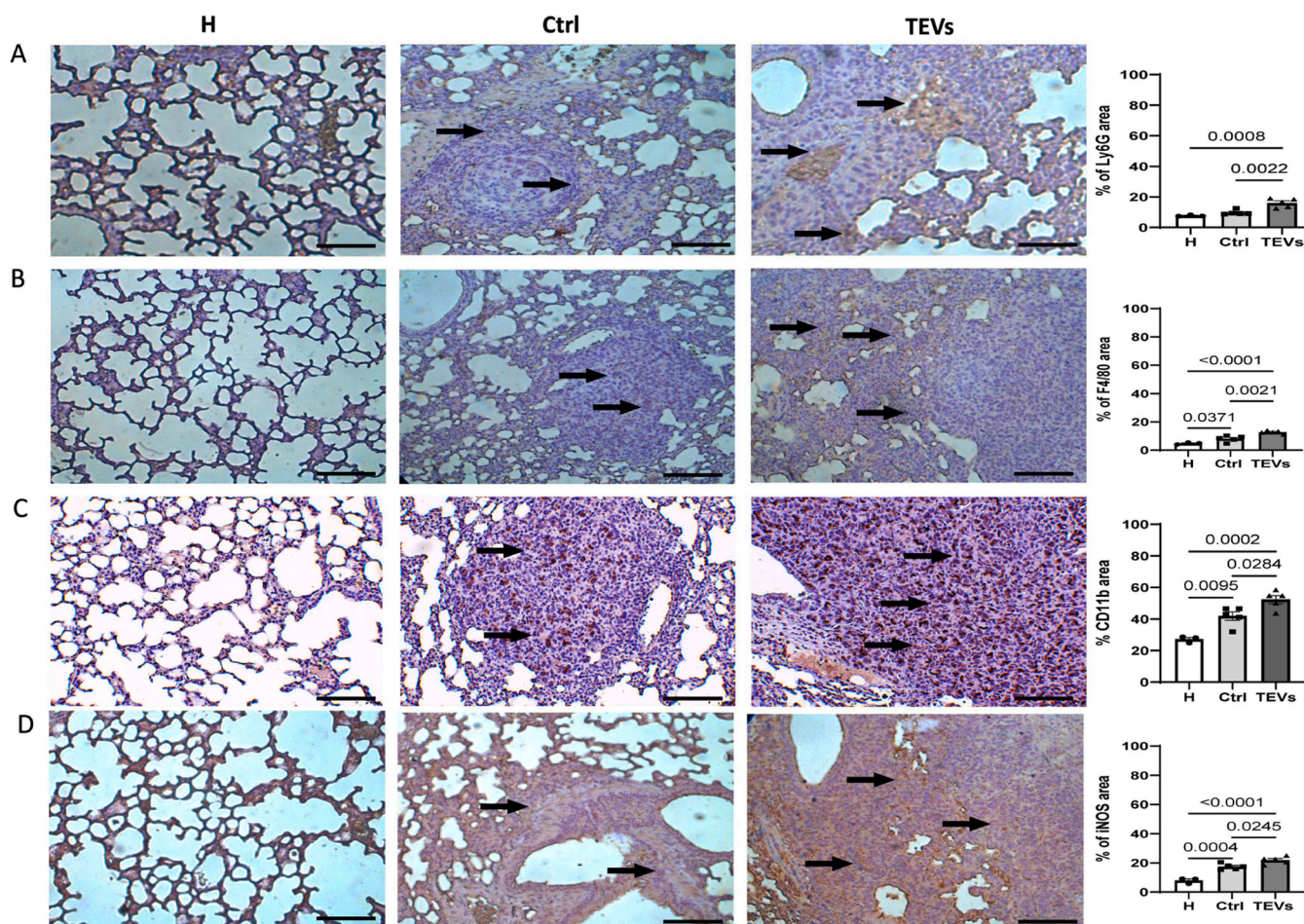
Fig. 6. Mice experiencing circulating TEVs display distinct inflammatory profiles in the lung. Representative immunohistochemistry analysis of lung tissue obtained from healthy (H), saline (Ctrl) and TEV mice (TEVs). Anti-Ly6G (A), anti-F4/80 (B), anti-CD11b (C), and anti-iNOS antibodies were used for the staining (D). Original magnification 20X, scale bar: 100 μm. Diagram data are presented as the mean ± SEM (n = 3 for healthy, n = 5 for experimental groups).

G-CSF, its content was also evaluated. No G-CSF was detected in TEVs (data not shown), while its level was significantly high in the CM of TEVs-pre-conditioned PBMCs (Fig. 9B). Finally, to exclude the possibility that EVs released by PBMCs upon TEVs-preconditioning may contain G-CSF, CM depleted of EVs was analysed for G-CSF content. Again, G-CSF was only detected in the CM but not in EVs (Fig. 9C), suggesting that, TEVs, rather than transfer their G-CSF content, induce its release from myeloid cells. The impact of G-CSF on the immunosuppressive compartments was further investigated by analysing CD11b$^+$ cells in co-culture condition before and after G-CSF blockade. As shown in Fig. 9E-F, CD11b$^+$ cell accumulation was significantly reduced upon G-CSF blockade.

3.6. TEV-enriched in mTOR contribute to G-CSF release and tumour immune suppression

TEVs deliver messages *via* their miRNA and protein cargoes to promote tumour progression [35]. Super-resolution microscopy was performed on 3 representative TEV samples confirming the EV size and the expression of the classical exosomal markers such as CD63, CD9 and CD81. As shown in Fig. 10A, TEVs are heterogeneous and all the combination of exosomal markers were detectable. Using TEV miRNAome analysis (Supplementary Table 1), we selected the top 35 miRNAs enriched in TEVs (RQ>10) for pathway and network-cluster analysis of miRNA target genes (Supplementary Table S2). Consistent with *in vivo* and *in vitro* results the immune system regulation was found as one of the most enriched pathways clustered into the 3 network communities

(Fig. 10B). Details of the "signal transduction and immune system regulation" community is shown in Fig. 10C and reported as gene-pathway network analysis in Supplementary Table S3. These observations strongly support the immunomodulatory properties of TEV-miRNA content, without providing a clear-cut information on the miRNAs specifically involved in. Thereby, based on TEV action on MDSCs, potential target protein(s) has been searched. Indeed, MDSC accumulation has been correlated with the Akt–mTOR in different tumour models [36,37], and more recently mTOR-G-CSF pathway has been recognized as crucial for MDSC accumulation [38]. Evaluating mTOR TEV content, we demonstrated that it was significantly enriched (Fig. 10D). Conversely, consistent with the failure of circulating EVs recovered from patients without cancer to increase lung metastases, mTOR was not detected (Supplementary Fig. S6). mTOR was also undetectable in EVs released from normal endothelial cells recovered from umbilical cord (data not shown). To further validate the potential contribute of mTOR in mediating TEV biological response, PBMCs either pre-treated or untreated with rapamycin and subjected to TEV administration were analysed for the phosphorylation of the mTOR down-stream target, S6 ribosomal protein [39]. As shown in Fig. 10E, S6 ribosomal protein underwent phosphorylation at Ser235/236 upon TEV treatment and rapamycin prevented its phosphorylation (Fig. 10E). These observations prompted us to investigate the effect of rapamycin in mediating G-CSF release. To this end, rapamycin was used during PBMC preconditioning and in co-cultures. Of note, we found that rapamycin significantly reduces TEVs-mediated G-CSF release in both experimental conditions (Fig. 11A-B). Moreover, an increase of human G-CSF was also
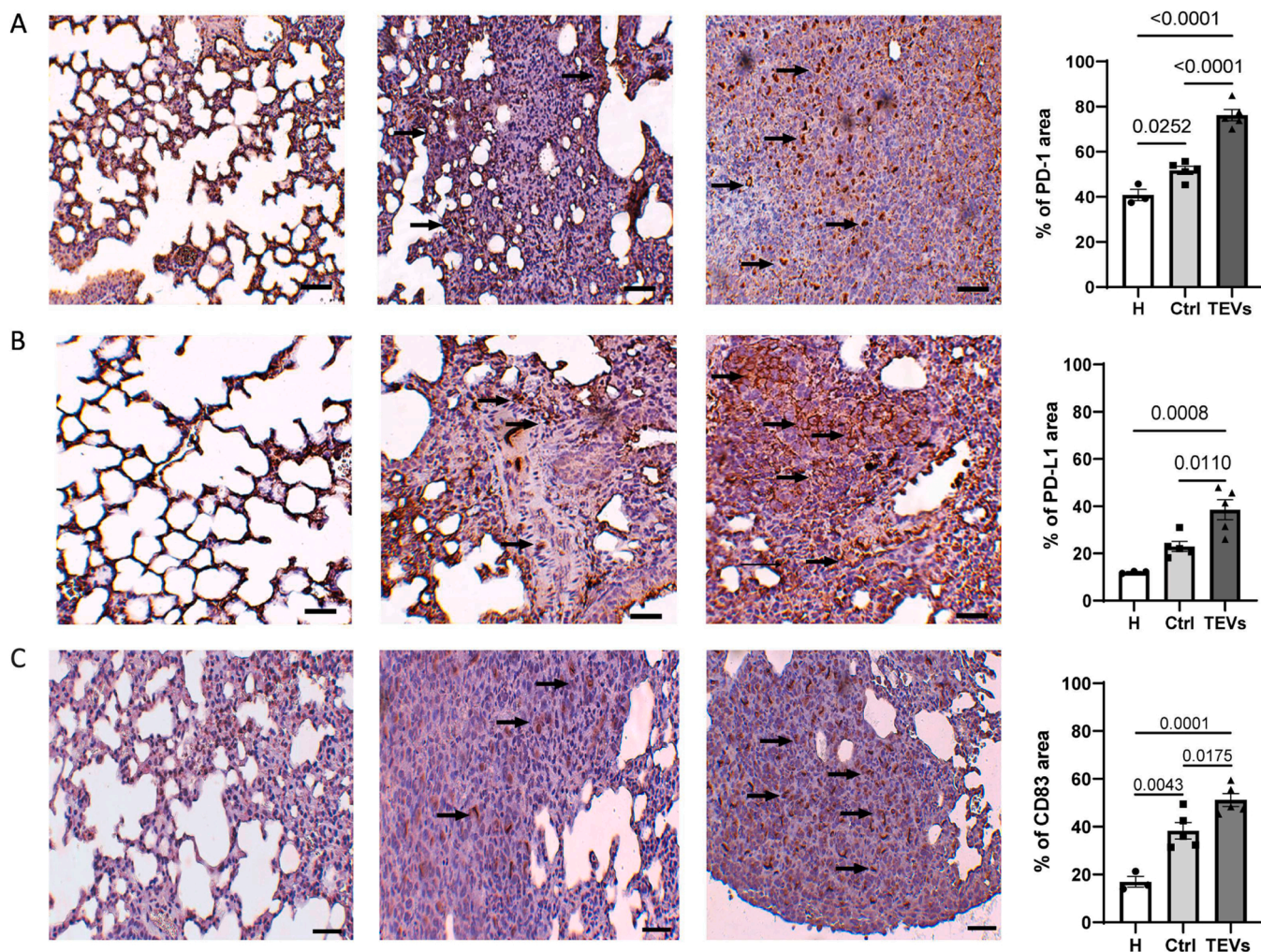
Fig. 7. Circulating TEVs induce PD-1/PD-L1 expression in lung. Representative immunohistochemistry analysis of lung tissue obtained from healthy (H), saline (Ctrl) and TEV mice (TEVs) stained with anti-PD-1 (A) anti-PD-L1 (B) and CD83 (C). Original magnification 20X, scale bar: 100 μm. Diagram data are presented as the mean ± SEM (n = 3 for healthy, n = 5 for experimental groups).

detected in co-culture experiments in the absence of TEVs, indicating that the crosstalk between PBMCs and cancer cells activates signals accounting for G-CSF release.

The release of G-CSF from cancer cells has been also reported [40, 41]. Therefore, the ability of TEV mTOR cargo to contribute to G-CSF release by cancer cells was analysed. As shown in Fig. 11, the release of G-CSF by cancer cells was not increased by TEVs, and as expected rapamycin was ineffective (Fig. 11C). By contrast, in TEVs-preconditioned PBMCs co-cultured with cancer cells a significant increase of murine G-CSF was detected, and rapamycin rescued the effect of PBMC-preconditioning on murine G-CSF release (Fig. 11D). Overall, these data support the notion that the interplay between cancer cells and PBMCs provides additional signals accounting for both cancer cells and PBMC-mediated G-CSF release, further boosted by TEVs.

4. Discussion

In the present study we first demonstrated that circulating EVs derived from tumour endothelial cells (TEVs), but not circulating EVs from patients without cancer, boosted neo-vessel formation and metastatic growth in the lung. Moreover, we found that TEVs induced a strong systemic and local immune reaction. Specifically, we demonstrated that circulating TEVs expand the population of Ly6G$^+$/F4/80$^-$/CD11b$^+$ cells in the spleen, bone marrow, and lung, while Ly6G$^+$/F4/

80$^+$/CD11b$^+$ in the spleen and lung. Moreover, we demonstrated that circulating TEVs were effective in inducing the expression of PD-1 and PD-L1 in the tumour setting. In the *in vitro* studies the expansion of CD11$^+$ cells and the exhaustion of T-cells exposed to TEVs were also demonstrated. Finally, mTOR- TEV content was found to induce the phosphorylation of its target S6 (Ser235/236) and the release of G-CSF by myeloid cells which, on turn, results in CD11$^+$ cell expansion. Overall, this study identifies circulating TEVs as instrumental to sort out a wide spectrum of immunosuppressive actions allowing the outgrowth of lung metastases.

Dynamic changes in tumour are mainly orchestrated inside the TME by the crosstalk among mesenchymal stem cells, cancer associated fibroblasts, endothelial cells, and immune cells [2]. Immune cells in the TME include innate (neutrophils, dendritic cells, macrophages, natural killer cells and MDSCs) and adaptive immune cells (T- and B cells) [42]. In this study, we provide evidence for the contribute of circulating TEVs in hijacking the local and systemic immune system to favour immune suppression and tumour outgrowth. More importantly, we provide evidence that circulating TEVs generate a systemic and local pro-tumour immune reaction involving both the innate and adaptive immune response. MDSCs and T-lymphocytes are indeed among the most relevant populations involved in evasion from immune-surveillance [42]. It has been extensively demonstrated that MDSC immunosuppressive mechanisms rely on TGFβ release, production of NO and ROS, and
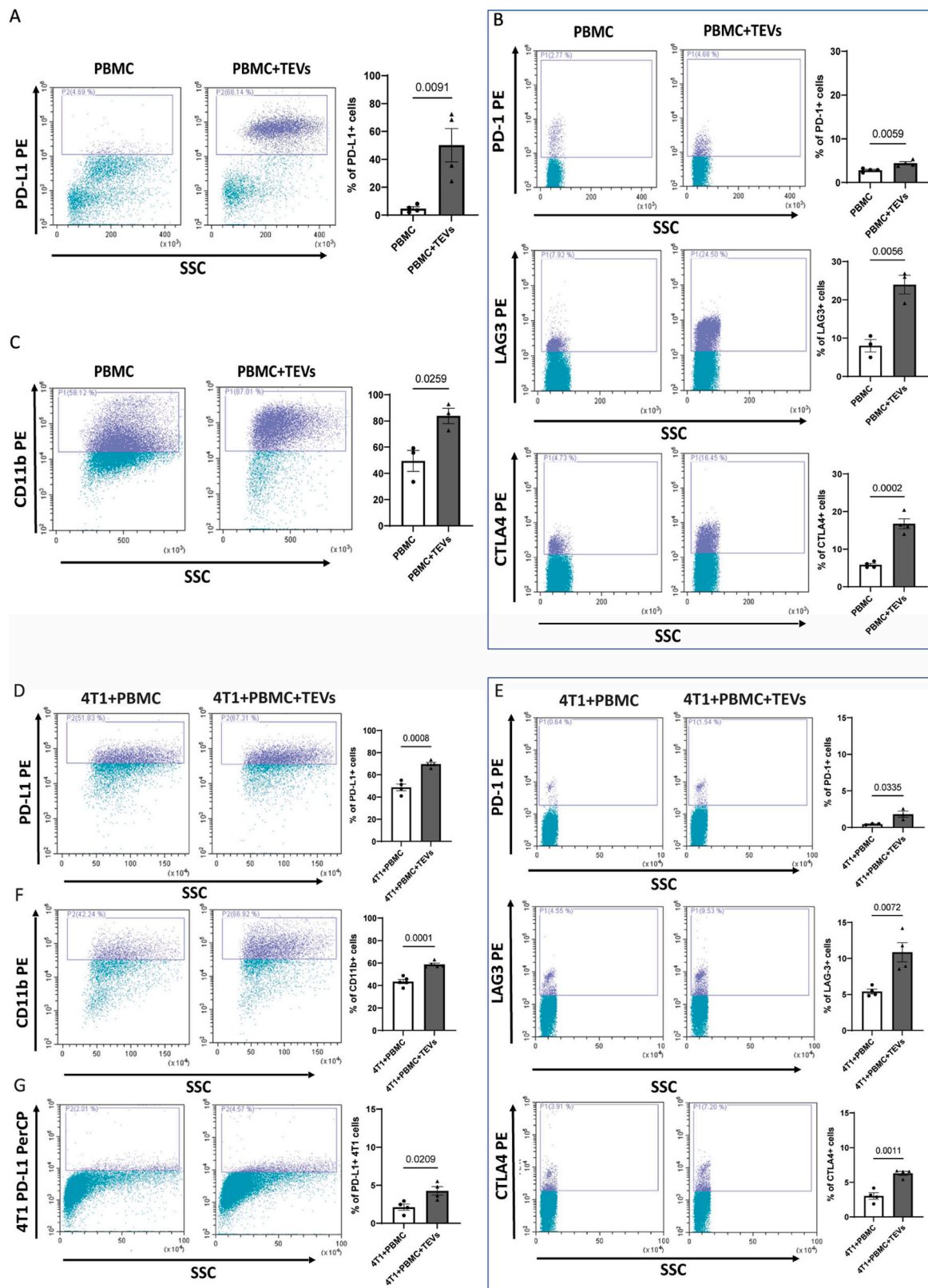
Fig. 8. TEVs drive an immune suppressive milieu involving both innate and adaptive immune cells. (A-B) Human PBMCs were treated or not with TEVs for 48 h and analysed by FACS. Representative FACS analysis of PD-L1$^+$ (gated on myeloid population), and PD-1$^+$, LAG3$^+$, and CTLA4$^+$ cells (gated on lymphocytes population). (C) Representative FACS analysis of CD11b$^+$ (gated on myeloid population) as indicated. (D-E) Human TEVs-preconditioned PBMC were co-cultured with 4T1 cells. Representative FACS analysis of PD-L1$^+$ (gated on myeloid population) and PD-1$^+$, LAG3$^+$, and CTLA4$^+$ cells (gated on lymphocytes population) were also evaluated. (F) Representative FACS analysis of CD11b$^+$ (gated on myeloid population). (G) Representative FACS analysis of murine PD-L1$^+$ cells. Diagram data are presented as the mean ± SEM (n = 3 or n = 4).
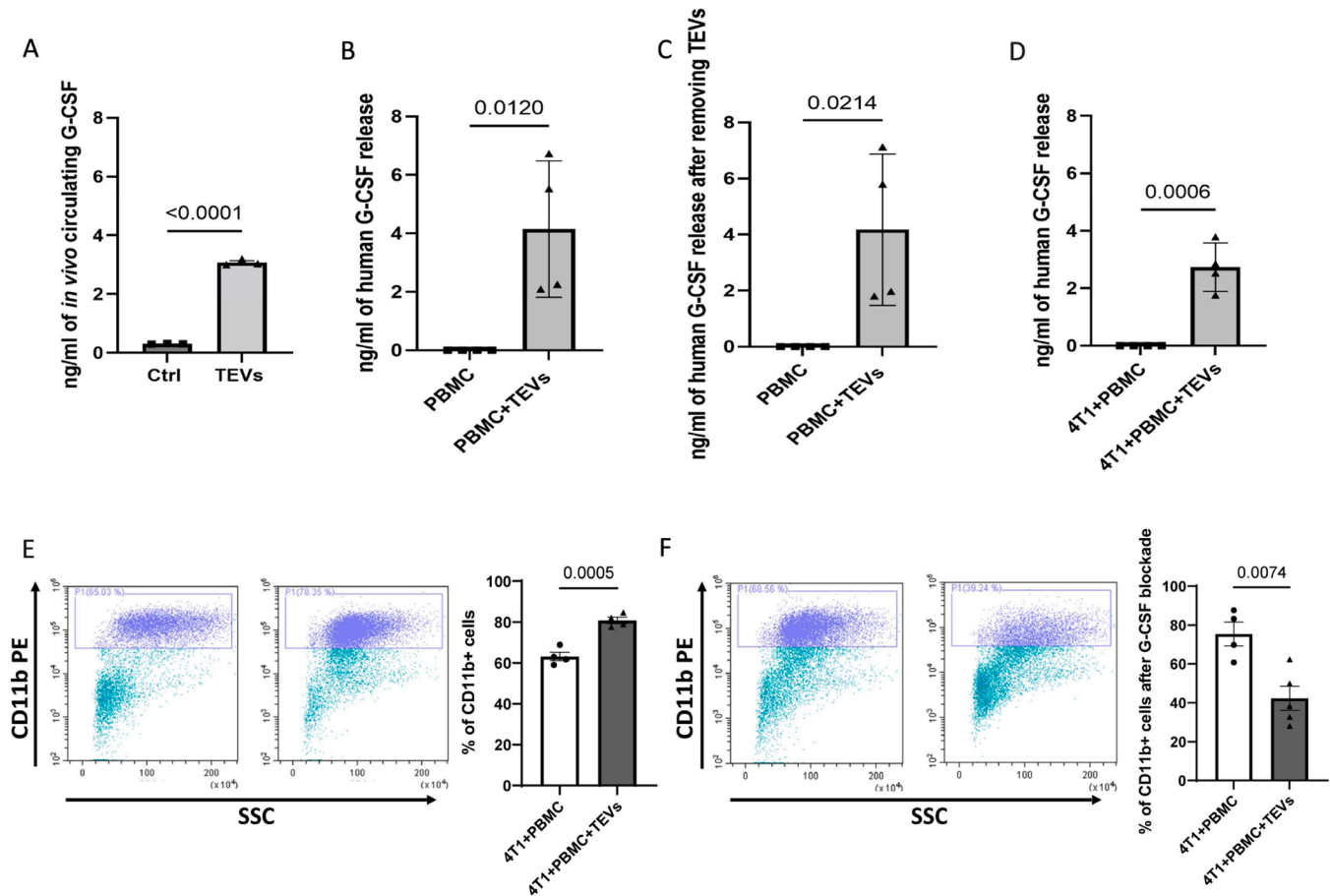
Fig. 9. G-CSF is increased both *in vivo* and *in vitro*. (A) Relative level of circulating G-CSF *in vivo*. Sera from control (Ctrl) and TEV mice (TEVs) were recovered to detect murine G-CSF. (n = 3) (B) Supernatants of PBMCs preconditioned with TEVs were analysed for G-CSF by ELISA (n = 4) (C) Supernatants of PBMCs pre-conditioned with TEVs were analysed for G-CSF after removing TEVs. (n = 4) (D) Supernatants of PBMCs preconditioned with TEVs co-cultured with 4T1 cells for 48 h were analysed for G-CSF by ELISA. (n = 4) (E-F) Representative FACS analysis of CD11b$^+$ cells (gated on myeloid population) before and after human G-CSF blockade. (n = 4 for control, n = 5 for TEVs). Diagram data are presented as the mean ± SEM.

depletion of L-arginine [43]. Consistent with the role of NO in MDSC accumulation immunohistochemical analysis demonstrated that Ly6G$^+$, F4/80$^+$, CD11b$^+$ cells and iNOS are increased in lung metastases generated by circulating TEVs. Moreover, NOS and ROS generation was associated with the increase of CD11b$^+$ cells when healthy PBMCs were preconditioned with TEVs or co-cultured with cancer cells.

FACS analysis of cells recovered from different organs demonstrated an increase of Ly6G$^+$/F4/80$^-$/CD11b$^+$ and Ly6G$^+$/F4/80$^+$/CD11b$^+$ cells in the spleen and in the lung metastases generated by TEVs, while only Ly6G$^+$/F4/80$^-$/CD11b$^+$ cells in the bone marrow. This suggests that in the bone marrow, circulating TEVs mainly contribute to the commitment of a specific myeloid compartment. G-CSF is recognized from among cytokines contributing to the expansion and bone marrow mobilization of MDSCs in cancer settings resulting in tumor angiogenesis, immune suppression, and tumor progression [44,45]. We herein demonstrated that G-CSF was increased in animals experiencing circulating TEVs. An increased G-CSF release was also found *in vitro* when PBMCs were stimulated with TEVs and when TEV-preconditioned PBMCs were co-cultured with tumour cells. Since TEVs are enriched of proteins and genetic materials [46], we first evaluated G-CSF in TEVs. Consistent with data obtained by Tkach et al. [47], we failed to detect G-CSF in TEVs. Moreover, no G-CSF was found in EVs released by PBMCs pre-conditioned with TEVs, indicating that PBMCs are the most relevant source of G-CSF when get in touch with TEVs or cancer cells. Moreover, consistent with the role of G-CSF in expanding CD11b$^+$ cells, we demonstrated that G-CSF blockade was able to reduce the percentage of

CD11b$^+$ positive cells either in TEVs-preconditioned PBMCs or in co-culture experiments.

Tumour cells by themselves are mostly involved in driving immunosuppression and in dictating their shift into cancer stem cells to accomplish their outgrowth and spread by releasing G-CSF [6]. Indeed, we demonstrated that cancer cells produce G-CSF, while TEVs have no additional effects. However, when cancer cells were co-cultured with TEVs-preconditioned PBMCs an increase of murine G-CSF was detected. This suggests that the amount of circulating G-CSF can both reflect the crosstalk between cancer cells and immune cells, and the ability of TEVs to trigger immune cells to release G-CSF.

Ly6G$^+$ CD11b$^+$ cells could secrete IL-1β to support angiogenesis, tumour cell dissemination, and immune suppression [48]. Indeed, animals exposed to TEVs are featured by the presence of Ly6G$^+$ CD11b$^+$ cells, and an increased network of vessels in the lung. Moreover, we demonstrated that IL-1β and IL-10 were increased in TEV-preconditioned PBMC co-cultured with cancer cells. Thereby we can speculate that besides on G-CSF, the impairment of the antitumor immune response may also relay on TEVs-mediated IL-1β [49] and IL-10 release [50]. However, since in immune-deficient models the proangiogenic and immune suppressive properties of TEVs were described as mediated by a specific miR package, it is most reasonable that the transfer of the entire TEV cargoes can contribute to vessel formation and tumour evasion in animals exposed to circulating TEVs.

The immunosuppressive network arranged by MDSCs in tumour setting is complex and involves a variety of immune cells including

Fig. 10. Network analysis of miRNA TEV content and mTOR TEV cargo (A) Representative super-resolution microscopy images of TEVs showing triple (CD63, CD81 and CD9) and double (CD9/CD81 and CD63/CD81) tetraspaning expression; CD63 appears in green, CD81 in red and CD9 in pink. The scale bares are below each EV image (50 nm/100 nm). Lower panel: clustering analysis of super-resolution microscopy images showing the single, double, and triple positive EV fractions. The analyses were performed in 3 EV preparations using CODI software; the graph shows the mean ± SD of a cumulative analysis of 3 fields for each preparation. (B-C) The pathway network and cluster analysis show the miRNA target genes-related pathways include the top 35 miRNAs enriched in TEC EVs. Node size is proportional to − log(q-value) of each pathway. Thickness of connections is proportional to the number of overlapping genes. Gene-pathway network analysis show pathways enriched in "immune system" cluster. Gene-nodes representing the genes enriched in each specific pathway are connected to pathway-nodes of origin. (D) Representative western blot analysis showing mTOR content in TECs and TEVs. CD29 and CD63 were used as exosomal marker, while GM130 served as negative exosomal marker. (E) Representative western blot analysis of p-S6 (Ser235/2369) in PBMCs 30 min treated with TEVs in the presence or in the absence of rapamycin. Anti-vinculin antibody was used as housekeeping protein (left panel). The histogram reports changes in S6 (Ser 235/236) phosphorylation in response to the indicated treatment (n = 3).

adaptive immune cells [6]. Several evidence indicates that MDSCs act as a powerful suppressor of T-cell activities to mediate tumour immune escape [6,7]. *In vivo*, we found that the increase of MDSCs was not associated with changes in CD3$^+$, CD8$^+$ or CD4$^+$ cells. However, when the expression of inhibitory receptors was analysed, animals experiencing circulating TEVs displayed and increased number of PD-L1, PD-1 and CD83 positive cells in the lung. Consistent with this observation, *in vitro* studies demonstrated that TEVs generate an immune suppressive milieu engaging T-cells, myeloid cells, and cancer cells expressing PD-1, CTLA4, LAG3, and PD-L1.

Tumour derived EVs move into circulation and reach distant sites to induce tumour progression also acting on immune cell reprogramming [35]. In the present study we provide evidence that also circulating TEVs may reach different tissues to expand specific immune suppressor cells. TEVs action relies on their specific cargoes, and major breakthrough in dissecting their role have unveiled as their miR content is crucial to reprogram the transcriptome of target cells [51]. We and other have reported in immune-deficient animals that a specific miR package drives tumour outgrowth also involving the expression of PD-L1 [18,52]. miR-10a [53], miR-21 [54], miR-29a [55], miR-92a [55] miR-107 [56], miR-155 [57], and miR-1246 [58] are among EV miRNAs involved in immunosuppression in many tumour types. Almost all these miRs are included in TEV cargo, and pathway and network-cluster analyses of miR target genes, obtained by selecting the most TEV-expressed miRs, demonstrated that the immune system regulation was one of the most enriched pathways clustered into the 3 network communities. This suggests that TEVs just transferring their miRNAs can act as strong immunomodulatory tumour arm. However, since these results have

been obtained only by bioinformatic analysis, additional information are required to further validate these observations. Nevertheless, recently Akt–mTOR signalling and mTOR-G-CSF pathway have been reported as crucial regulators of MDSC accumulation [36,37]. Therefore, since MDSCs accumulate in different organs, G-CSF was found increased *in vivo* and *in vitro,* and G-CSF was found crucial for the expansion of CD11$^+$ cells*,* we investigated the possibility that a specific TEV protein cargo may also impact this process. Of note, we demonstrated that, unlike circulating EVs from patients without tumour, TEVs are enriched in mTOR and *in vitro* they were able to phosphorylate the mTOR downstream target [39]. Consistently, mTOR inhibition abrogated the phosphorylation of the S6 ribosomal protein at Ser235/236 in PBMCs treated with TEVs and reduced, without completely abrogating, the release of G-CSF by both PBMCs preconditioned with TEVs or in co-culture with cancer cells. Overall, these observations, besides demonstrating that TEV-mTOR cargo grants for G-CSF release, further support the impact of the entire TEV cargo in rearranging the anti-tumour immune response. Finally, although sera from TEV-animals are enriched in anti-TEV antibodies, our study demonstrated that circulating TEVs are still able to hijack the immune system.

In conclusion, this study highlights the impact of circulating TEVs in inducing a strong local and systemic immune reaction and in dictating the fate of tumour by reprogramming immune cells to inhibit rather than boosting the anti-tumour immune response. This on turn translates into a favourable "soil" letting tumour forming vessels and grow. We also provide evidence that the release of G-CSF, at least mediated by mTOR-TEV cargo, impacts on the rearrangement of the immune system. Finally, since TEVs are worthy referred as tumour biomarkers and we

Fig. 11. mTOR TEV-content is involved in G-CSF release. (A) Supernatants of PBMCs preconditioned with TEVs were analysed for human G-CSF in the presence of 50 nM rapamycin. Untreated cells were used as control. (n = 3 or n = 4) (B) Supernatants of PBMCs preconditioned with TEVs co-cultured with 4T1 cells for 48 h were analysed for human G-CSF by ELISA upon 50 nM rapamycin. (n = 3 or n = 4) (C) Supernatants of 4T1 cells were analysed for murine G-CSF in the presence or absence of 50 nM rapamycin. (n = 6) (D) Supernatants of PBMCs preconditioned with TEVs co-cultured with 4T1 cells for 48 h were analysed for murine G-CSF in the presence or in the absence of 50 nM of rapamycin (n = 3 or n = 4). Diagram data are presented as the mean ± SEM.

failed to detect mTOR in circulating EVs from patients without cancer, we propose mTOR as an additional challenging circulating TEV marker and a potential predictor of tumour response to immunotherapeutic approaches.

CRediT roles

MK was involved in the *in vivo* experiments, and data curation. TL was involved in the *in vivo* experiments, and data curation. CG was involved in the *in vivo* experiments, and data curation. AS provided formal analysis of *in vitro* and *in vivo* experiments. MC performed the animal studies. SB provided formal analysis of *in vitro* experiments. FB performed bioinformatics analysis. SF isolated and characterized extracellular vesicles. GC revised the manuscript and performed TEM. MFB was involved in conceptualization, supervision, writing, review and editing the manuscript, as well as in providing resources. All authors revised the manuscript.

Declaration of Competing Interest

The other authors have no conflicts of interest to declare.

Data Availability

Data will be made available on request.

Appendix A. Supporting information

Supplementary data associated with this article can be found in the online version at doi:10.1016/j.phrs.2023.106871.

References

[1] M.A. Medina, G. Oza, A. Sharma, L.G. Arriaga, J.M. Hernández Hernández, V. M. Rotello, J.T. Ramirez, Triple-negative breast cancer: a review of conventional and advanced therapeutic strategies, Int. J. Environ. Res. Public Health 17 (2020), https://doi.org/10.3390/ijerph17062078.

[2] S. Maman, I.P. Witz, A history of exploring cancer in context, Nat. Rev. Cancer 18 (2018) 359–376, https://doi.org/10.1038/s41568-018-0006-7.

[3] L.T. Vu, B. Peng, D.X. Zhang, V. Ma, C.A. Mathey-Andrews, C.K. Lam, T. Kiomourtzis, J. Jin, L. McReynolds, L. Huang, A. Grimson, W.C. Cho, J. Lieberman, M.T. Le, Tumor-secreted extracellular vesicles promote the activation of cancer-associated fibroblasts via the transfer of microRNA-125b, J. Extracell. Vesicles 8 (2019) 1599680, https://doi.org/10.1080/20013078.2019.1599680.

[4] A. Ortiz, Extracellular vesicles in cancer progression, Semin. Cancer Biol. 76 (2021) 139–142, https://doi.org/10.1016/j.semcancer.2021.05.032.

[5] E. Vergani, E. Daveri, V. Vallacchi, L. Bergamaschi, L. Lalli, C. Castelli, M. Rodolfo, L. Rivoltini, V. Huber, Extracellular vesicles in anti-tumor immunity, Semin. Cancer Biol. 86 (2022) 64–79, https://doi.org/10.1016/j.semcancer.2021.09.004.

[6] V. Salemme, G. Centonze, F. Cavallo, P. Defilippi, L. Conti, The crosstalk between tumor cells and the immune microenvironment in breast cancer: implications for immunotherapy, Front. Oncol. 11 (2021), 610303, https://doi.org/10.3389/fonc.2021.610303.

[7] D. Moskophidis, F. Lechner, H. Pircher, R.M. Zinkernagel, Virus persistence in acutely infected immunocompetent mice by exhaustion of antiviral cytotoxic effector T cells, Nature 362 (1993) 758–761, https://doi.org/10.1038/362758a0.

[8] Z. Zhang, S. Liu, B. Zhang, L. Qiao, Y. Zhang, Y. Zhang, T cell dysfunction and exhaustion in cancer, Front. Cell Dev. Biol. 8 (2020) 17, https://doi.org/10.3389/fcell.2020.00017.

[9] J.S. Dolina, N. Van Braeckel-Budimir, G.D. Thomas, S. Salek-Ardakani, CD8(+) T cell exhaustion in cancer, Front. Immunol. 12 (2021), 715234, https://doi.org/10.3389/fimmu.2021.715234.

[10] M. Dysthe, R. Parihar, Myeloid-derived suppressor cells in the tumor microenvironment, Adv. Exp. Med. Biol. 1224 (2020) 117–140, https://doi.org/10.1007/978-3-030-35723-8_8.

[11] M.J. Hamilton, M. Bosiljcic, N.E. Lepard, E.C. Halvorsen, V.W. Ho, J.P. Banáth, G. Krystal, K.L. Bennewith, Macrophages are more potent immune suppressors ex vivo than immature myeloid-derived suppressor cells induced by metastatic murine mammary carcinomas, J. Immunol. 192 (2014) 512–522, https://doi.org/10.4049/jimmunol.1300096.

[12] Z. Xu, C. Guo, Q. Ye, Y. Shi, Y. Sun, J. Zhang, J. Huang, Y. Huang, C. Zeng, X. Zhang, Y. Ke, H. Cheng, Endothelial deletion of SHP2 suppresses tumor angiogenesis and promotes vascular normalization, Nat. Commun. 12 (2021) 6310, https://doi.org/10.1038/s41467-021-26697-8.

[13] B. Bussolati, I. Deambrosis, S. Russo, M.C. Deregibus, G. Camussi, Altered angiogenesis and survival in human tumor-derived endothelial cells, FASEB J.: Off. Publ. Fed. Am. Soc. Exp. Biol. 17 (2003) 1159–1161, https://doi.org/10.1096/fj.02-0557fje.

[14] I. Li, B.Y. Nabet, Exosomes in the tumor microenvironment as mediators of cancer therapy resistance, Mol. Cancer 18 (2019) 32, https://doi.org/10.1186/s12943-019-0975-5.

[15] G. Lombardo, M. Gili, C. Grange, C. Cavallari, P. Dentelli, G. Togliatto, D. Taverna, G. Camussi, M.F. Brizzi, IL-3R-alpha blockade inhibits tumor endothelial cell-derived extracellular vesicle (EV)-mediated vessel formation by targeting the β-catenin pathway, Oncogene 37 (2018) 1175–1191, https://doi.org/10.1038/s41388-017-0034-x.

[16] T. Lopatina, C. Grange, C. Cavallari, V. Navarro-Tableros, G. Lombardo, A. Rosso, M. Cedrino, M.A.C. Pomatto, M. Koni, F. Veneziano, I. Castellano, G. Camussi, M. F. Brizzi, Targeting IL-3Rα on tumor-derived endothelial cells blunts metastatic spread of triple-negative breast cancer via extracellular vesicle reprogramming, Oncogenesis 9 (2020) 90, https://doi.org/10.1038/s41389-020-00274-y.

[17] T. Lopatina, E. Favaro, L. Danilova, E.J. Fertig, A.V. Favorov, L.T. Kagohara, T. Martone, B. Bussolati, R. Romagnoli, R. Albera, G. Pecorari, M.F. Brizzi, G. Camussi, D.A. Gaykalova, Extracellular vesicles released by tumor endothelial cells spread immunosuppressive and transforming signals through various recipient cells, Front. Cell Dev. Biol. 8 (2020) 698, https://doi.org/10.3389/fcell.2020.00698.

[18] T. Lopatina, M. Koni, C. Grange, M. Cedrino, S. Femminò, G. Lombardo, E. Favaro, M.F. Brizzi, IL-3 signalling in the tumour microenvironment shapes the immune response via tumour endothelial cell-derived extracellular vesicles, Pharmacol. Res. (2022), 106206, https://doi.org/10.1016/j.phrs.2022.106206.

[19] C. Grange, B. Bussolati, S. Bruno, V. Fonsato, A. Sapino, G. Camussi, Isolation and characterization of human breast tumor-derived endothelial cells, Oncol. Rep. 15 (2006) 381–386.

[20] F. D'Ascenzo, S. Femminò, F. Ravera, A. Angelini, A. Caccioppo, L. Franchin, A. Grosso, S. Comità, C. Cavallari, C. Penna, G.M. De Ferrari, G. Camussi, P. Pagliaro, M.F. Brizzi, Extracellular vesicles from patients with Acute Coronary Syndrome impact on ischemia-reperfusion injury, Pharmacol. Res. 170 (2021), 105715, https://doi.org/10.1016/j.phrs.2021.105715.

[21] S. Femminò, F. D'Ascenzo, F. Ravera, S. Comità, F. Angelini, A. Caccioppo, L. Franchin, A. Grosso, C. Thairi, E. Venturelli, C. Cavallari, C. Penna, G.M. De Ferrari, G. Camussi, P. Pagliaro, M.F. Brizzi, Percutaneous coronary intervention (PCI) reprograms circulating extracellular vesicles from ACS patients impairing their cardio-protective properties, Int. J. Mol. Sci. 22 (2021), https://doi.org/10.3390/ijms221910270.

[22] R. Skovronova, C. Grange, V. Dimuccio, M.C. Deregibus, G. Camussi, B. Bussolati, Surface marker expression in small and medium/large mesenchymal stromal cell-derived extracellular vesicles in naive or apoptotic condition using orthogonal techniques, Cells 10 (2021), https://doi.org/10.3390/cells10112948.

[23] H. Dweep, C. Sticht, P. Pandey, N. Gretz, miRWalk–database: prediction of possible miRNA binding sites by "walking" the genes of three genomes, J. Biomed. Inform. 44 (2011) 839–847, https://doi.org/10.1016/j.jbi.2011.05.002.

[24] H.-Y. Huang, Y.-C.-D. Lin, J. Li, K.-Y. Huang, S. Shrestha, H.-C. Hong, Y. Tang, Y.-G. Chen, C.-N. Jin, Y. Yu, J.-T. Xu, Y.-M. Li, X.-X. Cai, Z.-Y. Zhou, X.-H. Chen, Y.-Y. Pei, L. Hu, J.-J. Su, S.-D. Cui, F. Wang, Y.-Y. Xie, S.-Y. Ding, M.-F. Luo, C.-H. Chou, N.-W. Chang, K.-W. Chen, Y.-H. Cheng, X.-H. Wan, W.-L. Hsu, T.-Y. Lee, F.-X. Wei, H.-D. Huang, miRTarBase 2020: updates to the experimentally validated microRNA-target interaction database, Nucleic Acids Res. 48 (2020) D148–D154, https://doi.org/10.1093/nar/gkz896.

[25] Z. Xie, A. Bailey, M.V. Kuleshov, D.J.B. Clarke, J.E. Evangelista, S.L. Jenkins, A. Lachmann, M.L. Wojciechowicz, E. Kropiwnicki, K.M. Jagodnik, M. Jeon, A. Ma'ayan, Gene set knowledge discovery with enrichr, Curr. Protoc. 1 (2021), e90, https://doi.org/10.1002/cpz1.90.

[26] V. Blondel, J.-L. Guillaume, R. Lambiotte, E. Lefebvre, Fast unfolding of communities in large networks, J. Stat. Mech. Theory Exp. 2008 (2008), https://doi.org/10.1088/1742-5468/2008/10/P10008.

[27] K. Tao, M. Fang, J. Alroy, G.G. Sahagian, Imagable 4T1 model for the study of late stage breast cancer, BMC Cancer 8 (2008) 228, https://doi.org/10.1186/1471-2407-8-228.

[28] S. Kreiser, J. Eckhardt, C. Kuhnt, M. Stein, L. Krzyzak, C. Seitz, C. Tucher, I. Knippertz, C. Becker, C. Günther, A. Steinkasserer, M. Lechmann, Murine CD83-positive T cells mediate suppressor functions in vitro and in vivo, Immunobiology 220 (2015) 270–279, https://doi.org/10.1016/j.imbio.2014.08.005.

[29] Z. Wu, T. Yoshikawa, S. Inoue, Y. Ito, H. Kasuya, T. Nakashima, H. Zhang, S. Kotaka, W. Hosoda, S. Suzuki, Y. Kagoya, CD83 expression characterizes precursor exhausted T cell population, Commun. Biol. 6 (2023) 258, https://doi.org/10.1038/s42003-023-04631-6.

[30] C. Lu, D. Zhou, Q. Wang, W. Liu, F. Yu, F. Wu, C. Chen, Crosstalk of MicroRNAs and oxidative stress in the pathogenesis of cancer, Oxid. Med. Cell. Longev. 2020 (2020) 2415324, https://doi.org/10.1155/2020/2415324.

[31] F. Weinberg, N. Ramnath, D. Nagrath, Reactive oxygen species in the tumor microenvironment: an overview, Cancers 11 (2019), https://doi.org/10.3390/cancers11081191.

[32] A. Luyckx, E. Schouppe, O. Rutgeerts, C. Lenaerts, S. Fevery, T. Devos, D. Dierickx, M. Waer, J.A. Van Ginderachter, A.D. Billiau, G-CSF stem cell mobilization in human donors induces polymorphonuclear and mononuclear myeloid-derived suppressor cells, Clin. Immunol. 143 (2012) 83–87, https://doi.org/10.1016/j.clim.2012.01.011.

[33] V.V. Malashchenko, M.E. Meniailo, V.A. Shmarov, N.D. Gazatova, O. B. Melashchenko, A.G. Goncharov, G.V. Seledtsova, V.I. Seledtsov, Direct anti-inflammatory effects of granulocyte colony-stimulating factor (G-CSF) on activation and functional properties of human T cell subpopulations in vitro, Cell. Immunol. 325 (2018) 23–32, https://doi.org/10.1016/j.cellimm.2018.01.007.

[34] A.J. Theron, H.C. Steel, B.L. Rapoport, R. Anderson, Contrasting immunopathogenic and therapeutic roles of granulocyte colony-stimulating factor in cancer, Pharmaceuticals 13 (2020), https://doi.org/10.3390/ph13110406.

[35] T. Lopatina, A. Sarcinella, M.F. Brizzi, Tumour derived extracellular vesicles: challenging target to blunt tumour immune evasion, Cancers 14 (2022), https://doi.org/10.3390/cancers14164020.

[36] M. Zhang, L. Wang, W. Liu, T. Wang, F. De Sanctis, L. Zhu, G. Zhang, J. Cheng, Q. Cao, J. Zhou, A. Tagliabue, V. Bronte, D. Yan, X. Wan, G. Yu, Targeting inhibition of accumulation and function of myeloid-derived suppressor cells by artemisinin via PI3K/AKT, mTOR, and MAPK pathways enhances Anti-PD-L1 immunotherapy in melanoma and liver tumors, J. Immunol. Res. 2022 (2022) 2253436, https://doi.org/10.1155/2022/2253436.

[37] S. Tohumeken, R. Baur, M. Böttcher, A. Stoll, R. Loschinski, K. Panagiotidis, M. Braun, D. Saul, S. Völkl, A.S. Baur, H. Bruns, A. Mackensen, R. Jitschin, D. Mougiakakos, Palmitoylated proteins on AML-derived extracellular vesicles promote myeloid-derived suppressor cell differentiation via TLR2/Akt/mTOR signaling, Cancer Res. 80 (2020) 3663–3676, https://doi.org/10.1158/0008-5472.CAN-20-0024.

[38] T. Welte, I.S. Kim, L. Tian, X. Gao, H. Wang, J. Li, X.B. Holdman, J.I. Herschkowitz, A. Pond, G. Xie, S. Kurley, T. Nguyen, L. Liao, L.E. Dobrolecki, L. Pang, Q. Mo, D. P. Edwards, S. Huang, L. Xin, J. Xu, Y. Li, M.T. Lewis, T. Wang, T.F. Westbrook, J. M. Rosen, X.H.-F. Zhang, Oncogenic mTOR signalling recruits myeloid-derived suppressor cells to promote tumour initiation, Nat. Cell Biol. 18 (2016) 632–644, https://doi.org/10.1038/ncb3355.

[39] O.H. Iwenofu, R.D. Lackman, A.P. Staddon, D.G. Goodwin, H.M. Haupt, J.S. J. Brooks, Phospho-S6 ribosomal protein: a potential new predictive sarcoma marker for targeted mTOR therapy, Mod. Pathol.: Off. J. U. S. Can. Acad. Pathol. Inc. 21 (2008) 231–237, https://doi.org/10.1038/modpathol.3800995.

[40] K.A. Mouchemore, R.L. Anderson, Immunomodulatory effects of G-CSF in cancer: Therapeutic implications, Semin. Immunol. 54 (2021), 101512, https://doi.org/10.1016/j.smim.2021.101512.

[41] I. Karagiannidis, E. Salataj, E. Said Abu Egal, E.J. Beswick, G-CSF in tumors: Aggressiveness, tumor microenvironment and immune cell regulation, Cytokine 142 (2021), 155479, https://doi.org/10.1016/j.cyto.2021.155479.

[42] K.J. Hiam-Galvez, B.M. Allen, M.H. Spitzer, Systemic immunity in cancer, Nat. Rev. Cancer 21 (2021) 345–359, https://doi.org/10.1038/s41568-021-00347-z.

[43] P. De Cicco, G. Ercolano, A. Ianaro, The new era of cancer immunotherapy: targeting myeloid-derived suppressor cells to overcome immune evasion, Front. Immunol. 11 (2020) 1680, https://doi.org/10.3389/fimmu.2020.01680.

[44] F. Shojaei, X. Wu, X. Qu, M. Kowanetz, L. Yu, M. Tan, Y.G. Meng, N. Ferrara, G-CSF-initiated myeloid cell mobilization and angiogenesis mediate tumor refractoriness to anti-VEGF therapy in mouse models, Proc. Natl. Acad. Sci. USA 106 (2009) 6742–6747, https://doi.org/10.1073/pnas.0902280106.

[45] M. Kowanetz, X. Wu, J. Lee, M. Tan, T. Hagenbeek, X. Qu, L. Yu, J. Ross, N. Korsisaari, Z. Cao, H. Bou-Reslan, D. Kallop, R. Weimer, M.J.C. Ludlam, J. S. Kaminker, Z. Modrusan, N. van Bruggen, F.V. Peale, R. Carano, Y.G. Meng, N. Ferrara, Granulocyte-colony stimulating factor promotes lung metastasis through mobilization of Ly6G+Ly6C+ granulocytes, Proc. Natl. Acad. Sci. USA 107 (2010) 21248–21255, https://doi.org/10.1073/pnas.1015855107.

[46] A. Becker, B.K. Thakur, J.M. Weiss, H.S. Kim, H. Peinado, D. Lyden, Extracellular vesicles in cancer: cell-to-cell mediators of metastasis, Cancer Cell 30 (2016) 836–848, https://doi.org/10.1016/j.ccell.2016.10.009.

[47] M. Tkach, J. Thalmensi, E. Timperi, P. Gueguen, N. Névo, E. Grisard, P. Sirven, F. Cocozza, A. Gouronnec, L. Martin-Jaular, M. Jouve, F. Delisle, N. Manel, D. C. Rookhuizen, C.L. Guerin, V. Soumelis, E. Romano, E. Segura, C. Théry, Extracellular vesicles from triple negative breast cancer promote pro-inflammatory macrophages associated with better clinical outcome, Proc. Natl. Acad. Sci. USA 119 (2022), e2107394119, https://doi.org/10.1073/pnas.2107394119.

[48] C. Rébé, F. Ghiringhelli, Interleukin-1β and cancer, Cancers 12 (2020), https://doi.org/10.3390/cancers12071791.

[49] S.K. Bunt, P. Sinha, V.K. Clements, J. Leips, S. Ostrand-Rosenberg, Inflammation induces myeloid-derived suppressor cells that facilitate tumor progression, J. Immunol. 176 (2006) 284–290, https://doi.org/10.4049/jimmunol.176.1.284.

[50] M. Moghimi, H. Ahrar, M. Karimi-Zarchi, K. Aghili, M. Salari, M. Zare-Shehneh, H. Neamatzadeh, Association of IL-10 rs1800871 and rs1800872 polymorphisms with breast cancer risk: a systematic review and meta-analysis, Asian Pac. J. Cancer Prev.: APJCP 19 (2018) 3353–3359, https://doi.org/10.31557/APJCP.2018.19.12.3353.

[51] M.-S. Njock, T. O'Grady, O. Nivelles, M. Lion, S. Jacques, M. Cambier, S. Herkenne, F. Muller, A. Christian, C. Remacle, J. Guiot, S. Rahmouni, F. Dequiedt, I. Struman, Endothelial extracellular vesicles promote tumour growth by tumour-associated macrophage reprogramming, J. Extracell. Vesicles 11 (2022), e12228, https://doi.org/10.1002/jev2.12228.

[52] V. Fleming, X. Hu, C. Weller, R. Weber, C. Groth, Z. Riester, L. Hüser, Q. Sun, V. Nagibin, C. Kirschning, V. Bronte, J. Utikal, P. Altevogt, V. Umansky, Melanoma extracellular vesicles generate immunosuppressive myeloid cells by upregulating PD-L1 via TLR4 signaling, Cancer Res. 79 (2019) 4715–4728, https://doi.org/10.1158/0008-5472.CAN-19-0053.

[53] X. Guo, W. Qiu, Q. Liu, M. Qian, S. Wang, Z. Zhang, X. Gao, Z. Chen, H. Xue, G. Li, Immunosuppressive effects of hypoxia-induced glioma exosomes through myeloid-derived suppressor cells via the miR-10a/Rora and miR-21/Pten Pathways, Oncogene 37 (2018) 4239–4259, https://doi.org/10.1038/s41388-018-0261-9.

[54] X. Zhang, F. Li, Y. Tang, Q. Ren, B. Xiao, Y. Wan, S. Jiang, miR-21a in exosomes from Lewis lung carcinoma cells accelerates tumor growth through targeting PDCD4 to enhance expansion of myeloid-derived suppressor cells, Oncogene 39 (2020) 6354–6369, https://doi.org/10.1038/s41388-020-01406-9.

[55] X. Guo, W. Qiu, J. Wang, Q. Liu, M. Qian, S. Wang, Z. Zhang, X. Gao, Z. Chen, Q. Guo, J. Xu, H. Xue, G. Li, Glioma exosomes mediate the expansion and function of myeloid-derived suppressor cells through microRNA-29a/Hbp1 and microRNA-92a/Prkar1a pathways, Int. J. Cancer 144 (2019) 3111–3126, https://doi.org/10.1002/ijc.32052.

[56] W. Ren, X. Zhang, W. Li, Q. Feng, H. Feng, Y. Tong, H. Rong, W. Wang, D. Zhang, Z. Zhang, S. Tu, X. Zhu, Q. Zhang, Exosomal miRNA-107 induces myeloid-derived suppressor cell expansion in gastric cancer, Cancer Manag. Res. 11 (2019) 4023–4040, https://doi.org/10.2147/CMAR.S198886.

[57] H. Bruns, M. Böttcher, M. Qorraj, M. Fabri, S. Jitschin, J. Dindorf, L. Busch, R. Jitschin, A. Mackensen, D. Mougiakakos, CLL-cell-mediated MDSC induction by exosomal miR-155 transfer is disrupted by vitamin D, Leukemia 31 (2017) 985–988, https://doi.org/10.1038/leu.2016.378.

[58] W. Qiu, X. Guo, B. Li, J. Wang, Y. Qi, Z. Chen, R. Zhao, L. Deng, M. Qian, S. Wang, Z. Zhang, Q. Guo, S. Zhang, Z. Pan, S. Zhao, H. Xue, G. Li, Exosomal miR-1246 from glioma patient body fluids drives the differentiation and activation of myeloid-derived suppressor cells, Mol. Ther.: J. Am. Soc. Gene Ther. 29 (2021) 3449–3464, https://doi.org/10.1016/j.ymthe.2021.06.023.